iScience

CellPress

Article

Longitudinal *In Vivo* Assessment of Host-Microbe Interactions in a Murine Model of Pulmonary Aspergillosis

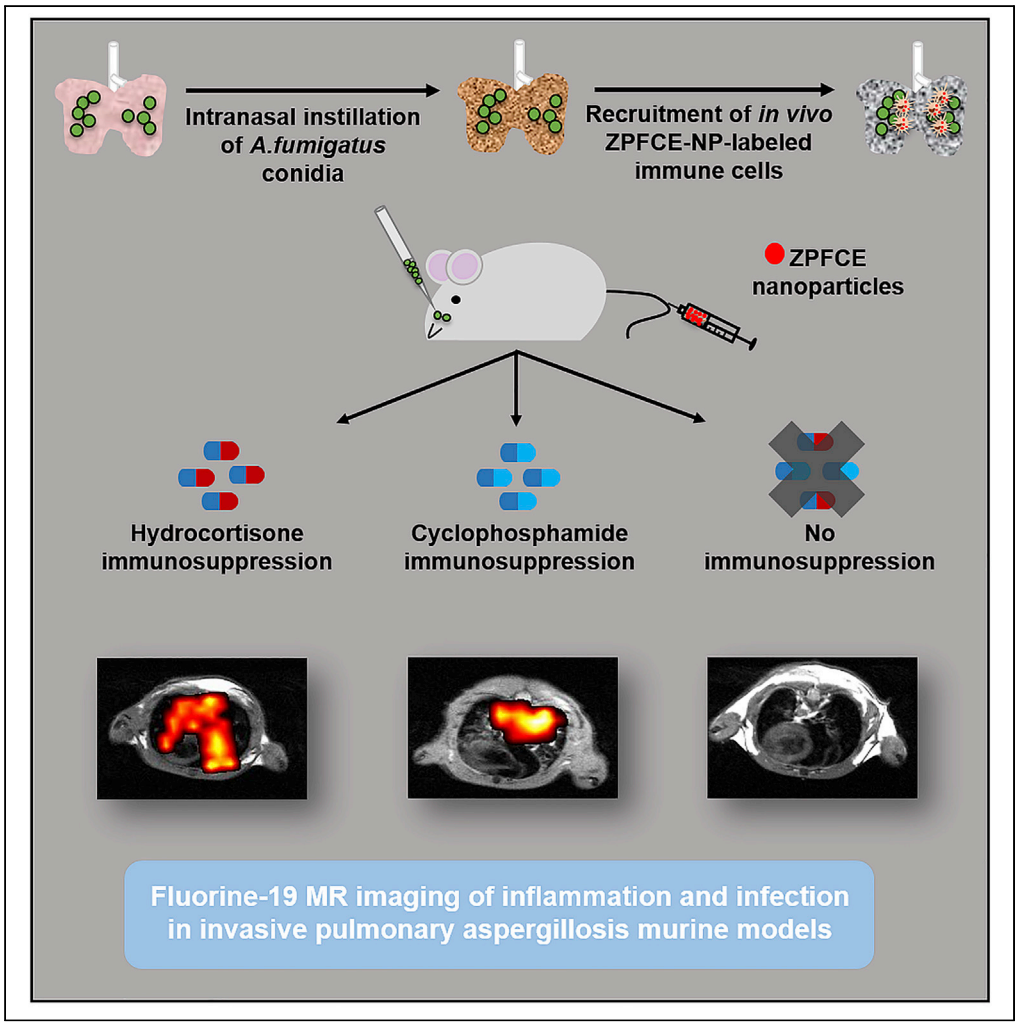

Shweta Saini, Jennifer Poelmans, Hannelie Korf, ..., Conny Gysemans, Stefaan C. De Smedt, Uwe Himmelreich

uwe.himmelreich@kuleuven.be

HIGHLIGHTS

Host-pathogen immune response is visualized *in vivo* and quantified against IPA

Modified PFC-based nanoparticles were used for *in vivo* labeling of immune cells

Clinical immunosuppression depict dynamic immune response upon fungal challenge

^{19}F MRI showed follow-up of labeled immune cells in individual animals over time

Saini et al., iScience *20*, 184–194
October 25, 2019
https://doi.org/10.1016/j.isci.2019.09.022

iScience

CellPress

Article

Longitudinal *In Vivo* Assessment of Host-Microbe Interactions in a Murine Model of Pulmonary Aspergillosis

Shweta Saini,[1] Jennifer Poelmans,[1] Hannelie Korf,[2] James L. Dooley,[3] Sayuan Liang,[1,4] Bella B. Manshian,[1] Rein Verbeke,[5] Stefaan J. Soenen,[1] Greetje Vande Velde,[1] Ine Lentacker,[5] Katrien Lagrou,[6] Adrian Liston,[3] Conny Gysemans,[7] Stefaan C. De Smedt,[5] and Uwe Himmelreich[1,8,*]

SUMMARY

The fungus *Aspergillus fumigatus* is ubiquitous in nature and the most common cause of invasive pulmonary aspergillosis (IPA) in patients with a compromised immune system. The development of IPA in patients under immunosuppressive treatment or in patients with primary immunodeficiency demonstrates the importance of the host immune response in controlling aspergillosis. However, study of the host-microbe interaction has been hampered by the lack of tools for their non-invasive assessment. We developed a methodology to study the response of the host's immune system against IPA longitudinally *in vivo* by using fluorine-19 magnetic resonance imaging (^{19}F MRI). We showed the advantage of a perfluorocarbon-based contrast agent for the *in vivo* labeling of macrophages and dendritic cells, permitting quantification of pulmonary inflammation in different murine IPA models. Our findings reveal the potential of ^{19}F MRI for the assessment of rapid kinetics of innate immune response against IPA and the permissive niche generated through immunosuppression.

INTRODUCTION

Aspergillus fumigatus is an opportunistic, potentially life-threatening fungus, which thrives mainly on organic substrates like decaying vegetation in the soil or food. Although environmental exposure of humans to the airborne *A. fumigatus* conidia is common, host-pathogen interactions effectively eradicate conidia from the pulmonary region of healthy individuals (Margalit and Kavanagh, 2015; Mccormick et al., 2010). The key determinant of infection is thought to be the innate immune response. *A. fumigatus* conidia in the alveolar space of lungs trigger pathogen recognizing receptors (PRRs), driving the first responders of the immune system (Dagenais and Keller, 2009). Key cellular mediators of immunity include resident alveolar macrophages, monocytes and dendritic cells for the engulfment of conidia, and neutrophils for the destruction of hyphae using neutrophil extracellular traps (Khanna et al., 2016; Roilides et al., 1998; Sales-campos et al., 2013; Zhang et al., 2019).

Healthy individuals effectively clear *A. fumigatus*, whereas infection becomes life-threatening in immunocompromised patients. With an increasing number of immunocompromised patients from organ transplantation or cancer treatment, invasive pulmonary aspergillosis (IPA) is rapidly growing as a medical problem (Berenguer et al., 1995). The acute inflammation in the lungs of patients with IPA suggests an underlying malfunction, rather than absence, of essential host immune components as the causative factor (Krenke and Grabczak, 2011). The *modus operandi* for the clinical use of immunosuppressive drugs mainly includes cyclophosphamide (CY) (Emadi et al., 2009) and hydrocortisone acetate (HCA) (Garth and Steele, 2017; Shaikh et al., 2012) administered intravenously to the patients. In previous studies, it was shown that the pathophysiology of IPA and the immune response against the fungal infection differs for each compounds (Dagenais and Keller, 2009; Stephens-Romero et al., 2005). Corticosteroids treatment impairs phagocyte function, including an abnormality in cellular migration and production of the inflammatory cytokines, while leaving neutrophils intact and functional (Brummer et al., 2001; Kamberi et al., 2002; Nawada et al., 1996). The phagocytic defect permits infection growth, which in turn drives a massive recruitment of neutrophils to the site of infection, resulting in intensive tissue damage. By contrast, CY induces neutropenia and depletes other circulating white blood cells, while leaving the local innate immune response relatively intact. Here the neutropenia is thought to be critical in permitting hyphal growth and further invasion

[1]Biomedical MRI/Molecular Small Animal Imaging Center (MoSAIC), KU Leuven, Leuven, Belgium

[2]Laboratory of Hepatology, CHROMETA Department, KU Leuven, Leuven, Belgium

[3]Laboratory of Genetics of Autoimmunity (VIB-KU Leuven Center for Brain & Disease Research), Leuven, Belgium

[4]Philips Research China, Shanghai, China

[5]Ghent Research Group on Nanomedicines, Ghent University, Belgium

[6]Clinical Bacteriology and Mycology, Department of Microbiology and Immunology, KU Leuven, Leuven, Belgium

[7]Clinical and Experimental Endocrinology, KU Leuven, Leuven, Belgium

[8]Lead Contact

*Correspondence: uwe.himmelreich@kuleuven.be

https://doi.org/10.1016/j.isci.2019.09.022

in the tissue (Jones et al., 2019; Kalleda et al., 2016). A key limitation of these conclusions, however, is the reliance on invasive methods that are restricted to single time point measurements, such as immunohistochemistry (Balloy et al., 2005; Wang et al., 2017). Knowledge of immune kinetics and longitudinal disease progression is currently lacking but is essential for understanding the dynamics of these processes (Kalleda et al., 2016). *In vivo* imaging techniques are potentially able to assess the host response against the infection longitudinally in individual animals.

Different imaging techniques have been used in preclinical models to characterize IPA, such as computed tomography, positron emission tomography, bioluminescence imaging, single photon emission tomography, proton magnetic resonance imaging (^{1}H MRI), and fibered confocal fluorescence microscopy (Brock et al., 2008; Poelmans et al., 2016, 2018; Rolle et al., 2016; Vanherp et al., 2018; Wang et al., 2013). Although these approaches fulfill the non-invasive and longitudinal criteria required, they lack specific information on inflammatory processes occurring in the host. In other disease models, *ex vivo* and *in vivo* cell labeling approaches use ^{1}H MRI contrast agents to visualize immune cells for studying various inflammatory processes (De Temmerman et al., 2014; Ho and Hitchens, 2004; Schwarz et al., 2012; Wu et al., 2006). However, ^{1}H MRI contrast agents such as (super)paramagnetic nanoparticles generate unspecific signal voids, making it difficult to locate and quantify labeled cells *in vivo*. Fluorine contrast agents in combination with ^{19}F MRI may provide an alternative, with specific and quantifiable contrast (Ebner et al., 2010; Srinivas et al., 2010a; Zhong et al., 2015).

^{19}F MRI is an emerging non-invasive tool, which can be applied both for imaging of *ex vivo* contrast agent labeled cells after their transplantation and for *in vivo* labeling of cells after systemic administration of fluorinated contrast agents (Jacoby et al., 2014b; Srinivas et al., 2012, 2010b). Using fluorinated contrast agents such as perfluoro-15-crown-5-ether nanoparticles (PFCE-NPs) in combination with ^{19}F MRI, one can generate highly specific MR contrast, owing to the lack of background signal. Overlaying the ^{19}F MR image with a conventional ^{1}H MR image provides the necessary anatomical background (Liang et al., 2018).

Here, we developed an imaging platform allowing non-invasive and longitudinal quantification of the degree of pulmonary inflammation in IPA murine models. We showed that the *in vivo* labeling of immune cells with newly developed zonyl perfluoro-15-crown-5-ether nanoparticles (ZPFCE-NPs) reveal underlying pathophysiological events during acute IPA using ^{19}F MRI.

RESULTS

Small-Sized Biocompatible ZPFCE-NPs Showed Efficient *In Vitro* Labeling of Murine Phagocytes

To monitor the immune responses *in vivo*, we sought to exploit the functional property of phagocytosis for immune cells labeling. ZPFCE-NPs label professional phagocytic cells owing to their small size (Waiczies et al., 2011). To validate the feasibility of this strategy, Macrophages, identified by their characteristic high surface expression of CD11b and F4/80, successfully phagocytosed ZPFCE-NPs in a dose-dependent manner (Figure 1). ZPFCE-NP labeling of macrophages showed similar labeling efficiencies for particle concentrations of 1 and 10 mM (Figure 1A). We used ZPFCE-NPs incorporated with Cholesteryl BODIPY FLC 12 green fluorescent dye. These nanoparticles did not show nanotoxicity in primary macrophages upon labeling with relatively high concentrations, affirming their suitability for *in vivo* applications (Figure S1).

A key requirement for an *in vivo* labeling protocol is that the label does not interfere with the biological processes being measured. To investigate whether ZPFCE-NP labeling modulates macrophage function, we tested key innate and adaptive functions *in vitro*. Using cytokine secretion as a readout for innate functional activation of macrophages, we found no impact of ZPFCE-NPs on spontaneous or lipopolysaccharide (LPS)-induced immune activation at a dose of 1 mM and only a weak enhancement of LPS-induced TNF-alpha production at 10 mM (Figure 2A). For the adaptive immune system, we tested the biological effect of ZPFCE-NPs labeling on antigen-presentation by macrophages. C57BL/6 peritoneal macrophages were pre-labeled with ZPFCE-NPs and pulsed with OVA peptide (OVA323-339) before co-culture with OVA-reactive OT-II TCR transgenic CD4+ T cells. OT-II T cells showed efficient activation when primed with OVA-loaded macrophages, which was unaltered by the pre-loading with ZPFCE-NPs (Figure 2B). Together, these results demonstrate that 1 mM ZPFCE-NPs allow macrophage labeling without inducing biological alterations to either the innate or adaptive functions of macrophages.

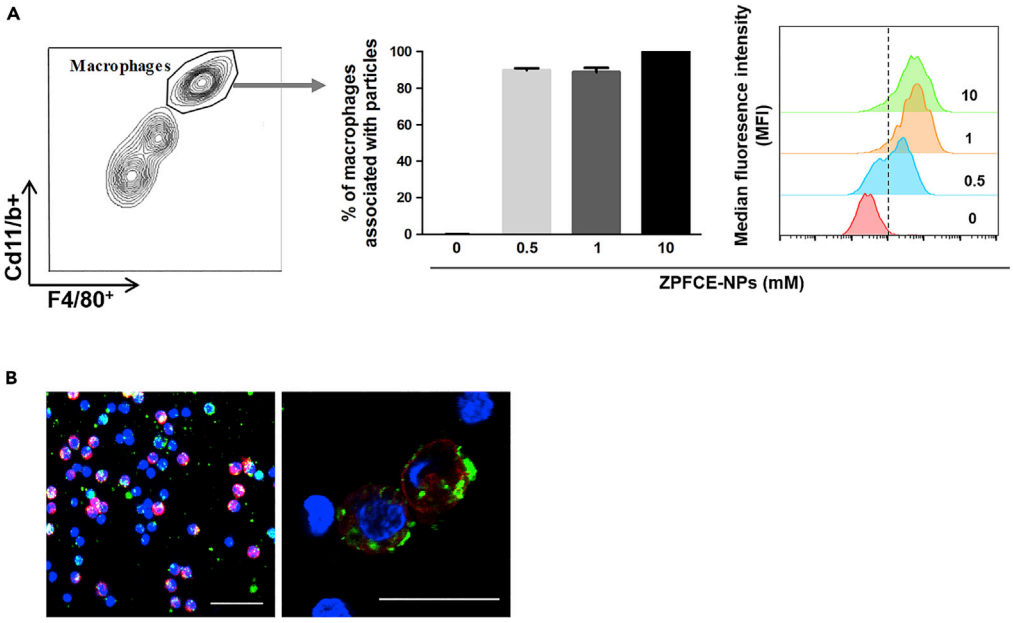

Figure 1. ZPFCE-NPs Allow Labeling of Macrophages

(A) Labeling of macrophages (positive cells for F4/80 and CD11b surface marker) with ZPFCE-NPs was measured in terms of percentage uptake at variable doses of particles. Median fluorescence intensities were measured from the gated ZPFCE-NP-labeled macrophages for each dose (mean ± SD).

(B) Confocal image showing macrophages stained by F4/80 surface (red) with the ZPFCE-NPs (green), magnified representative images show intracellular uptake of ZPFCE-NPs. Scale bar is 20μm.

^{19}F MRI Allows *In Vivo* Visualization and Quantification of Immune Cell Recruitment in *A. fumigatus*-Infected Lungs

Having validated ZPFCE-NPs as an efficient and biologically neutral contrast agent for macrophages, we sought to assess the *in vivo* utility using IPA mouse models to apply our methodology as a proof of principle. To test the robustness of our immunomonitoring method, we used three models of pulmonary aspergillosis with immunocompetent and immunosuppressed mice, together with non-infected mice as control. CY or HCA immunosuppressive drugs were used to induce neutropenia and phagocytic dysfunction in mice, respectively. Immunocompetent mice infected with *A. fumigatus* demonstrated a large and rapid influx of macrophages into the lung within 4 h of infection (Figure 3A, second row and 3B). Inflammation was quickly resolved, with a return to near-baseline macrophage levels by 24 h (Figure 3B). By contrast, both forms of immunosuppression sharply reduced the immediate innate response to infection, with poor influx at 4 h (Figure 3A, third and fourth row and 3B). In both cases, this defect in the immediate response corrected with a more chronic inflammatory signal, with large macrophage influx out to at least 3 days post infection (Figure 3B), consistent with a model where the defective immediate response allowed infection to become invasive and chronic. We observed and quantified a higher fluorine MRI signal intensity in the HCA mice as compared with the CY mice groups at the site of inflammation post pulmonary infection. No detectable fluorine signal was observed from the non-infected immunocompetent mice (N-IC).

Key differences were also observed between the immunosuppressed groups, with HCA-treated mice but not CY-treated mice, resulting in a transient flux of macrophages into the cervical lymph nodes on day 1 post infection (Figure 3C). This indicates that HCA allows macrophage mobilization but diverts recruitment into the draining lymph node rather than into the tissue.

To monitor progression of infection, we applied a cumulative scoring of ^{1}H MR images based on the lung signal intensity in all murine groups. This shows the pathophysiological changes occurring over time following infection from day of infection (day 0) until day 3 (Figure S2A). We have observed high signal intensities in the CY group where infection was more profound compared with the HCA group (Figure S2B).

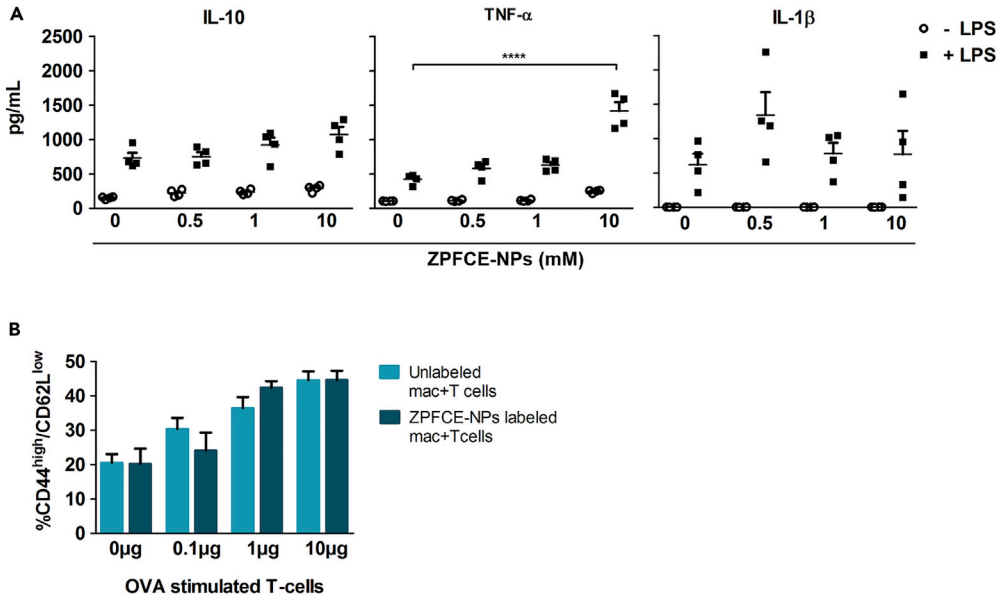

Figure 2. ZPFCE-NPs Allow Labeling of Murine Macrophages without Modulating Their Innate and Adaptive Immune Function

(A) Cytokine measurements performed on supernatants from ZPFCE-labeled macrophages in the presence and absence of LPS. Data represent mean ± SEM (n = 5, ****$p < 0.0001$).

(B) C57BL/6 peritoneal macrophages were pre-loaded with ZPFCE-NPs and pulsed with OVA peptide ($OVA_{323-339}$) at different concentrations, before co-culture with OT-II TCR transgenic CD4+ T cells. After 3 days of co-culture, the cells were stained for lineage T cell markers in combination with T cell activation markers and analyzed by flow cytometry. The percentage of $CD44^{high}CD62L^{low}$ activated T cells across variable doses of the OT-II peptide, for ZPFCE-NP-labeled and unlabeled macrophages (mean ± SEM).

Together, these results both validate ^{19}F MRI as an *in vivo* monitoring tool for anti-microbe responses and indicate a critical window of response for the innate immune system against *A. fumigatus* invasive infection.

Distinctive Fungal Burden Depicted by Bioluminescent Imaging and Colony-Forming Units Confirms Infection

To affirm infection and viable pulmonary fungal load with inflammatory processes that we have monitored by ^{19}F MRI, we have examined the $Fluc^+$ *A. fumigatus* infection 3 days after infection by using *ex vivo* bioluminescent imaging (BLI). After D-luciferin administration in the lungs, CY-treated mice showed higher BLI signal intensity compared with the hydrocortisone-treated mice (Figure 4A). No detectable bioluminescence signal was observed from the lungs in the two control groups, infected immunocompetent and non-infected mice. Quantification of BLI signal also showed significantly high fungal infection in the CY-treated group compared with the hydrocortisone-treated group and infected-immunocompetent group (Figure 4B). This indicates strong invasion of fungi in the lungs of the CY group owing to lack of an efficient immune response compared with the HCA group, where the immune response prevents the growth of *A. fumigatus*.

For the quantification of pulmonary fungal load, we performed colony-forming unit (CFU) counting on the cultured lung homogenates from all mice groups. We observed a significant increase in the *A. fumigatus* burden in the lungs of the CY group when compared with the HCA on day 3 (Figure 4C). In contrast, N-IC and I-IC groups did not show any fungal growth. These results together with ^{19}F MRI suggest the early immune activation in infected mice as a critical aspect for the control of potentially invasive *A. fumigatus* progression.

Validation of ZPFCE-NP-Labeled Immune Cell Recruitment in the Lungs and Lymph Nodes by Histology and Immunofluorescence Imaging

To validate our imaging results, we performed periodic acid-Schiff (PAS) staining and immunofluorescence after sacrificing the animals 3 days after infection. Similar to ^{19}F MRI, we observed high pulmonary

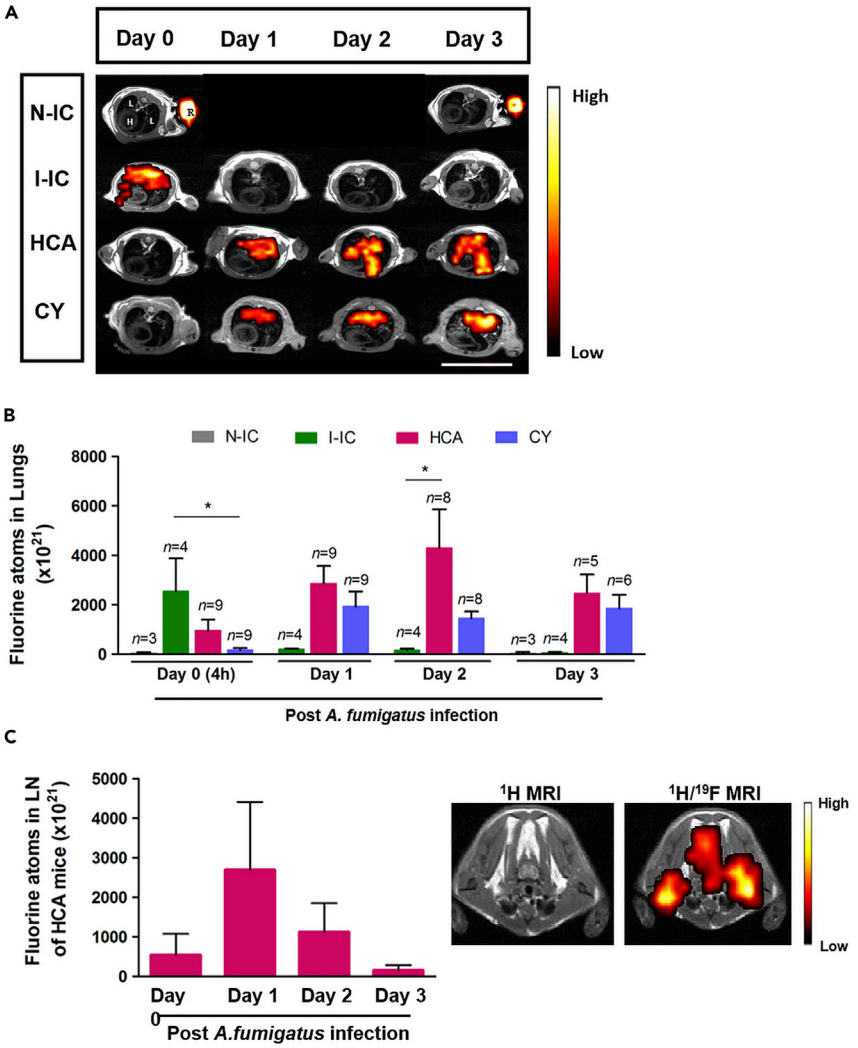

Figure 3. ^{19}F MRI Identifies the Differential Local Immune Response to Infection by *A. fumigatus* in Immunocompromised Murine Hosts

(A) ^{19}F MR images (fluorine signal was superimposed on anatomical ^{1}H MR images) were obtained from HCA, CY, and infected-immunocompetent (I-IC) mice as well as non-infected control mice (N-IC) on day 0 (4 h post infection). All mice received systemic injection of ZPFCE-NPs on day 0 (4 h post infection) and day 1. All infected mice were imaged daily (^{1}H and ^{19}F MRI). The non-infected immunocompetent (N-IC) group was followed up on day 0 and day 3. Labels for different organs (image top left) include H, heart; L, lungs; and R, reference containing 30 mM ZPFCE-NP. Scale bar is 2.6 cm.

(B) Quantification of the ^{19}F MR signal from the lung region was performed for all groups by comparing the signal intensity of the lung region with a reference (R in (A) top left image) containing 30 mM ZPFCE-NPs. Data shown as mean ± SEM (*$p < 0.05$).

(C) ^{19}F MRI signal was observed from the lymph node region only for mice from the HCA group on day 1. Mean ^{19}F MR signal intensity was quantified with respect to the 30 mM reference placed next to each animal. ^{19}F MRI signal in lymph nodes is indicated as hot spots overlaid over the anatomical ^{1}H MR image (right panel). Data shown as mean ± SEM (*$p < 0.05$).

inflammation in the lung tissue of the HCA group upon *A. fumigatus* challenge with minimal fungal invasion. In contrast, the CY group, showed as expected fungal growth and hyphal growth formation with invasion in nearby tissues and no visible inflammation (Figure 5A). The two control N-IC and I-IC mice groups showed normal lung tissue morphology with no fungal infection on day 3, validating the ^{19}F MRI findings.

Immunofluorescence images also showed the presence of stringent inflammation resulting in higher influx of ZPFCE-NP-labeled macrophages and dendritic cells in the lungs of the HCA group in contrast

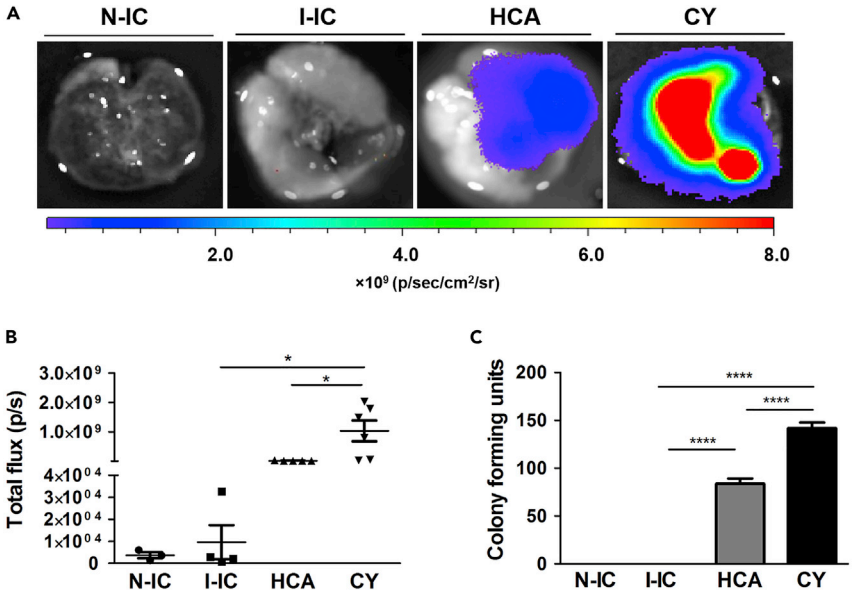

Figure 4. Visualization and Quantification of Fungal Load Reveals the Impaired Immune Response against *A. fumigatus* Invasion in Immunocompromised Mice

(A) *Ex vivo* bioluminescent imaging (BLI) was performed to visualize firefly luciferase (Fluc)-expressing *A. fumigatus* in the lungs 3 days after the infection. After the endpoint ^{19}F MRI experiment, animals were sacrificed and D-luciferin was administered into the excised lungs of murine groups of mice. Lungs were imaged immediately after D-luciferin administration. The scale bar represents BLI signal intensity in photons flux/second. The color-coded BLI images are overlaid onto the photographic images of lungs. Intensity thresholds for all BLI images were kept the same.

(B) BLI signal intensity from all murine groups was measured as total flux after assigning identical regions of interest on the BLI images of lungs.

(C) Lungs were isolated 3 days after infection from all mice groups. Colony-forming units (CFUs) were manually counted from lung homogenates 24 h after incubation at 37°C. No fungi were observed in the two control groups (N-IC and I-IC). Data are represented as mean ± SEM (*$p < 0.05$, ****$p < 0.0001$). HCA $n = 5$, CY $n = 6$, I-IC $n = 4$, N-IC $n = 3$.

to the CY group (Figure 5B, third and fourth row). Additionally, elevated recruitment of granulocytes was observed near the airways of the HCA group compared with other groups. The N-IC and I-IC groups showed no visible inflammation or infection similar to ^{19}F MRI (Figure 5B, first and second row). We also noticed differences in white blood cell counts, analyzed individually from the peripheral blood of different groups on day 3, indicating severe inflammation in the HCA group reflected by an increase in the number of neutrophils and lymphocytes in the blood in contrast to the CY group (Figure S3). The non-infected model showed similar levels of neutrophils and lymphocytes as the I-IC model where immune cells were in the normal range. Notably, the cervical lymph nodes of the HCA group showed high ZPFCE-NPs accumulation (Figure S4). ZPFCE-NPs were also visualized in the OCT (optimum cutting temperature)-embedded lungs on day 3 by *ex vivo* fluorescence imaging illustrating high fluorescent signal observed both in the lungs and cervical lymph nodes, only in the HCA group (Figure S5). Briefly, these results strongly support the ^{19}F MRI findings, demonstrating the feasibility of our established methodology for non-invasive monitoring of infection.

DISCUSSION

With the increased number of immunocompromised patients, it becomes more important to closely monitor those patients, diagnose, and follow up IPA. Among the profound number of clinical IPA cases, 90% are caused by *A. fumigatus* (Lin et al., 2001; Massam et al., 2011). For a better understanding of aspergillosis and for testing of novel antifungal compounds, preclinical animal models are essential. Although methods for monitoring the dynamics of the immune cells upon *A. fumigatus* infection have been developed recently (Kalleda et al., 2016), these studies were not able to assess the interaction with the host's immune system longitudinally *in vivo*. Here, we have developed an approach that allows the non-invasive, dynamic monitoring of both inflammatory processes and the infection in three different animal models of IPA.

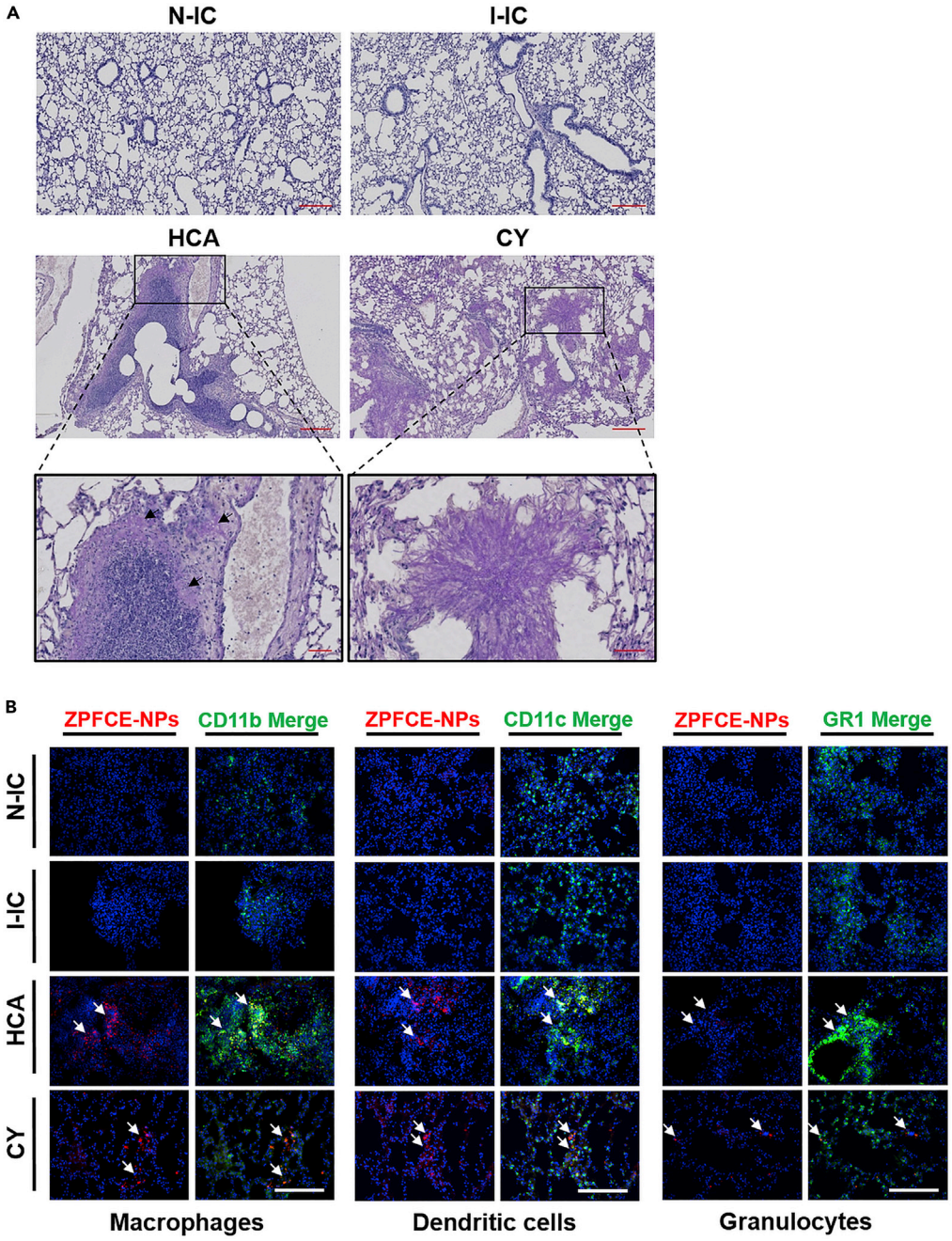

Figure 5. Histological Imaging Elucidates Diverse Infection and Inflammation Patterns in Immunocompromised Groups

(A) Representative light microscopy of PAS-stained images showing histopathology from the PFA fixed lung sections of different mice groups on day 3 post infection. Excessive immune cell infiltration near the bronchi and bronchiole upon pulmonary *A. fumigatus* infection in HCA mice showing profound inflammation-induced tissue destruction. Mild fungal infection observed in HCA mice (black arrows, HCA magnified image). Fungal dissemination shown in the CY mice resulted in compression of lung tissue with massive hyphal growth (magnified CY image). Scale bar is 200 μm for the first and second rows and 50 μm for magnified images (third row).

(B) Immunofluorescence microscopy performed on fresh-frozen lung tissues showing the ZPFCE-NP-labeled macrophages (anti CD11b) and dendritic cells (anti CD11c) recruited to the bronchioles (white arrows) in the lungs of HCA and CY mice. Granulocytes (anti-GR1) were also found to be accumulated (white arrows) in high numbers in the HCA group compared with other groups. Scale bar is 100 μm, and staining represented as Blue = DAPI, Red = ZPFCE-NPs.

Several cell-labeling approaches have been established to non-invasively visualize the mechanisms of immune reactions involved in various diseases by tracking the loci of inflammatory immune cells using ^{19}F MRI (Ebner et al., 2010; Flogel et al., 2008; Jacoby et al., 2014a; Stoll et al., 2012). In this study, we focused on the quantification and localization of inflammation in IPA murine models of immune impairments induced by clinically used immunosuppressive drugs (Balloy et al., 2005; Stergiopoulou et al., 2007; Woodruff and Hebert, 2002). PFCs have been used and tested as blood substitutes and thus proven to be safe in humans (Janjic and Ahrens, 2009; Ruiz-Cabello et al., 2011). Here, we synthesized ZPFCE-NPs and studied their potential for the labeling of phagocytic immune cells. It has been shown that labeling with PFCE particles of different sizes could potentially modulate the immune function of dendritic cells (Waiczies et al., 2011). In this study, we showed the biological compatibility of ZPFCE-NPs for *in vivo* studies, where labeled macrophages retained their antigen processing and T cell activation capacity. Compared with most other PFCs, ZPFCE-NPs have a reduced size of ~280 nm (Dewitte et al., 2013).In our *in vivo* study, we have used ^{19}F MRI to quantify inflammation non-invasively and longitudinally after systemic injections of ZPFCE-NPs. The ^{19}F MRI signal detected in inflamed areas corresponds to the infiltration of labeled phagocytic cells in the region of interest (Flogel et al., 2008; van Heeswijk et al., 2015). We observed high ^{19}F MRI signal intensities in the lungs of the infected immunocompetent (I-IC) mice already 4 h after the fungal infection, which was completely cleared after 24 h, confirming the expected eradication of *A. fumigatus* conidia by the immune system. In the hydrocortisone (HCA)-treated mice, the exacerbated intrusive recruitment of immune cells resulted in the labeling of not only tissue-resident macrophages but also dendritic cells (Temme et al., 2012). Inflammation was found to be less pronounced in the CY-treated mice, with increased fungal invasion in the lungs. We did not observe any detectable fluorine signal in the lungs from the non-infected immunocompetent (N-IC) mice that have received ZPFCE-NPs, indicating absence of any inflammation in the lungs. Only in HCA mice, elevated accumulation of ZPFCE-NPs was observed in the nearby cervical lymph nodes to 3 days after infection as shown in the ^{19}F MR images.

In addition to ^{19}F MRI, *in vivo* ^{1}H MRI in these mouse models was able to document the lesion development occurring in the lungs upon fungal conidia challenge. As shown by our quantitative image analysis, we observed high lung lesion formation in CY mice two and three days after infection, which is consistent with profound fungal hyphal growth and invasion in lungs as reported before (Poelmans et al., 2016). ^{1}H MRI indicated only weak lesion formation in the infected HCA-treated and I-IC groups. These results endorse the fact that the administration of CY as a frequently used immunosuppressive drug can lead to lethal IPA with mild initial inflammation in the lungs as indicated by ^{19}F MRI. On the contrary, hydrocortisone-based immunosuppression leads to less lesion formation by *A. fumigatus* but triggers acute inflammation leading to potentially lethal tissue destruction (Kalleda et al., 2016). The functional immune system of the infected-immunocompetent mice resulted in the rapid initial immune reaction and complete clearance of the fungi as shown in the ^{1}H MR images and also confirmed by histology. By using ^{19}F MRI, we were able to monitor the intricate dynamic profile of the host-pathogen interaction in pulmonary *A. fumigatus* infection *in vivo*. We documented the differences between immunocompetent hosts and animals treated with two different immunosuppressive compounds. With clinically safe contrast agents like perfluorocarbon (PFC)-based fluorinated nanoparticles, ^{19}F MRI not only proved to be a powerful imaging modality for numerous preclinical studies but also showed potential for translation to humans. For immune cell imaging, ^{19}F MRI has developed into a robust method for the follow-up of phagocytic cells with less success in the tracking of non-phagocytic cells owing to the sensitivity issues of ^{19}F MRI (Saini et al., 2019).

In summary, we demonstrated the potential of ^{19}F MRI and perfluorocarbon-based ZPFCE-NPs by successful tracking and quantifying the fluorine signal generated by innate immune cells, macrophages, and dendritic cells in the lungs corresponding to the intensity of local inflammation. By being able to monitor both the infection and immune reaction in live animals over time, it is possible to make treatment decisions rapidly and almost in real time. In the future, this will help in testing transgenic fungal strains, novel antifungal drugs, or new approaches to influence the immune system. Overall, it will provide an emerging ^{19}F MRI platform for studying not only basic mechanisms of fungal infections but also advanced immune cell therapies in patients (Ahrens et al., 2014; Amiri et al., 2015; Fink et al., 2018; Hertlein et al., 2013).

Limitations of the Study

Although the PFC-based fluorinated nanoparticles provided specific contrast for immune cell imaging in the preclinical aspergillosis models, ^{19}F MRI is still limited to applications where large cell numbers accumulate locally. For less severe models of inflammation, the sensitivity of ^{19}F MRI needs to be improved by

using either contrast agents with higher fluorine load or improved hardware (Khalil et al., 2019) and/or image processing approaches (Liang et al., 2017). In addition, *in vivo* cell labeling was restricted to phagocytic cells like macrophages. Animal models used in this study were already described by invasive methods. In the future, a comparative experiment using a PRR knockout mouse strain instilled with a transgenic fungus lacking a key PAMP (e.g., melanin or galactosaminoglycan) can be used as a suitable model to study the immune response in differently modulated transgenic animals.

METHODS

All methods can be found in the accompanying Transparent Methods supplemental file.

SUPPLEMENTAL INFORMATION

Supplemental Information can be found online at https://doi.org/10.1016/j.isci.2019.09.022.

ACKNOWLEDGMENTS

The authors acknowledge Dr. Bala Attili (Laboratory of Radiopharmaceutical Research, KU Leuven, Belgium) for providing help with the formulation of HCA treatment and Dr. Matthias Brock (University of Nottingham, UK) for providing the Fluc$^+$ *A. fumigatus* strain 2/7/1. Use of the strain was granted by the Leibniz Institute for Natural Product Research and Infection Biology (Hans Knöll Institute, Jena, Germany). We are grateful for the financial support by the following funding agencies: the European Commission Marie Curie (ITN) BetaTrain (289932), the Research Foundation Flanders (FWO, G.0A75.14, G.0B28.14, and G.069115N), the Agentschap voor Innovatie door Wetenschap en Technologie for the SBO NanoCoMIT (IWT SBO 140061), the European ERA-NET project "CryptoView" (third call of the FP7 programme Infect-ERA), and KU Leuven for PF 10/017 (IMIR).

AUTHOR CONTRIBUTIONS

Conceptualization, S.S. and U.H.; Methodology, S.S., H.K., J.P., J.L.D., B.B.M., S.J.S., S.L., R.V., I.L., and G.V.V.; Investigation, S.S., J.P., B.B.M., and H.K.; Writing - Original Draft, S.S.; Writing - Review & Editing, S.S., J.P., A.L., C.G., S.C.D., and U.H.; Funding Acquisition, U.H., S.C.D., H.K., G.V.V., I.L., and K.L.; Supervision, H.K. and U.H.

DECLARATION OF INTERESTS

The authors declare no competing interests.

Received: May 12, 2019
Revised: July 24, 2019
Accepted: September 13, 2019
Published: October 25, 2019

REFERENCES

Ahrens, E.T., Helfer, B.M., O'Hanlon, C.F., and Schirda, C. (2014). Clinical cell therapy imaging using a perfluorocarbon tracer and fluorine-19 MRI. Magn. Reson. Med. *72*, 1696–1701.

Amiri, H., Srinivas, M., Veltien, A., van Uden, M.J., de Vries, I.J.M., and Heerschap, A. (2015). Cell tracking using 19F magnetic resonance imaging: technical aspects and challenges towards clinical applications. Eur. Radiol. *25*, 726–735.

Balloy, V., Huerre, M., Latgé, J.-P., and Chignard, M. (2005). Differences in patterns of infection and inflammation for corticosteroid treatment and chemotherapy in experimental invasive pulmonary aspergillosis. Infect. Immun. *73*, 494–503.

Berenguer, J., Allende, M.C., Lee, J.W., Garrett, K., Lyman, C., Ali, N.M., Bacher, J., Pizzo, P.A., and Walsh, T.J. (1995). Pathogenesis of pulmonary aspergillosis: Granulocytopenia versus cyclosporine and methylprednisolone-induced immunosuppression. Am. J. Respir. Crit. Care Med. *152*, 1079–1086.

Brock, M., Jouvion, G., Droin-Bergère, S., Dussurget, O., Nicola, M.A., and Ibrahim-Granet, O. (2008). Bioluminescent *Aspergillus fumigatus*, a new tool for drug efficiency testing and in vivo monitoring of invasive aspergillosis. Appl. Environ. Microbiol. *74*, 7023–7035.

Brummer, E., Maqbool, A., and Stevens, D.A. (2001). In vivo GM-CSF prevents dexamethasone suppression of killing of *Aspergillus fumigatus* conidia by bronchoalveolar macrophages. J. Leukoc. Biol. *70*, 868–872.

Dagenais, T.R.T., and Keller, N.P. (2009). Pathogenesis of *Aspergillus fumigatus* in invasive aspergillosis. Clin. Microbiol. Rev. *22*, 447–465.

De Temmerman, M.-L., Soenen, S.J., Symens, N., Lucas, B., Vandenbroucke, R.E., Libert, C., Demeester, J., De Smedt, S.C., Himmelreich, U., and Rejman, J. (2014). Magnetic layer-by-layer coated particles for efficient MRI of dendritic cells and mesenchymal stem cells. Nanomedicine *9*, 1363–1376.

Dewitte, H., Geers, B., Liang, S., Himmelreich, U., Demeester, J., De Smedt, S.C., and Lentacker, I. (2013). Design and evaluation of theranostic perfluorocarbon particles for simultaneous antigen-loading and19F-MRI tracking of dendritic cells. J. Control Release *169*, 141–149.

Ebner, B., Behm, P., Jacoby, C., Burghoff, S., French, B.A., Schrader, J., and Flögel, U. (2010). Early assessment of pulmonary inflammation by 19F MRI in vivo. Circ. Cardiovasc. Imaging *3*, 202–210.

Emadi, A., Jones, R.J., and Brodsky, R.A. (2009). Cyclophosphamide and cancer: golden anniversary. Nat. Rev. Clin. Oncol. *6*, 638–647.

Fink, C., Gaudet, J.M., Fox, M.S., Bhatt, S., Viswanathan, S., Smith, M., Chin, J., Foster, P.J., and Dekaban, G.A. (2018). 19F-perfluorocarbon-labeled human peripheral blood mononuclear cells can be detected in vivo using clinical MRI parameters in a therapeutic cell setting. Sci. Rep. *8*, 590.

Flogel, U., Ding, Z., Hardung, H., Jander, S., Reichmann, G., Jacoby, C., Schubert, R., and Schrader, J. (2008). In vivo monitoring of inflammation after cardiac and cerebral ischemia by fluorine magnetic resonance imaging. Circulation *118*, 140–148.

Garth, J.M., and Steele, C. (2017). Innate lung defense during invasive aspergillosis: new mechanisms. J. Innate Immun. *9*, 271–280.

Hertlein, T., Sturm, V., Jakob, P., and Ohlsen, K. (2013). 19F magnetic resonance imaging of perfluorocarbons for the evaluation of response to antibiotic therapy in a staphylococcus aureus infection model. PLoS One *8*, e64440.

Ho, C., and Hitchens, T.K. (2004). A non-invasive approach to detecting organ rejection by MRI: monitoring the accumulation of immune cells at the transplanted organ. Curr. Pharm. Biotechnol. *5*, 551–566.

Jacoby, C., Borg, N., Heusch, P., Sauter, M., Bönner, F., Kandolf, R., Klingel, K., Schrader, J., and Flögel, U. (2014a). Visualization of immune cell infiltration in experimental viral myocarditis by 19F MRI in vivo. Magn. Reson. Mater. Phys. Biol. Med. *27*, 101–106.

Jacoby, C., Temme, S., Mayenfels, F., Benoit, N., Krafft, M.P., Schubert, R., Schrader, J., and Flögel, U. (2014b). Probing different perfluorocarbons for in vivo inflammation imaging by19F MRI: image reconstruction, biological half-lives and sensitivity. NMR Biomed. *27*, 261–271.

Janjic, J.M., and Ahrens, E.T. (2009). Fluorine-containing nanoemulsions for MRI cell tracking. Wiley Interdiscip. Rev. Nanomed. Nanobiotechnol. *1*, 492–501.

Jones, C.N., Ellett, F., Robertson, A.L., Forrest, K.M., Judice, K., Balkovec, J.M., Springer, M., Markmann, J.F., Vyas, J.M., Warren, H.S., and Irimia, D. (2019). Bifunctional small molecules enhance neutrophil activities against *Aspergillus fumigatus* in vivo and in vitro. Front. Immunol. *10*, 644.

Kalleda, N., Amich, J., Arslan, B., Poreddy, S., Mattenheimer, K., Mokhtari, Z., Einsele, H., Brock, M., Heinze, K.G., and Beilhack, A. (2016). Dynamic immune cell recruitment after murine pulmonary *Aspergillus fumigatus* infection under different immunosuppressive regimens. Front. Microbiol. *7*, 1–15.

Kamberi, M., Brummer, E., and Stevens, D.A. (2002). Regulation of bronchoalveolar macrophage proinflammatory cytokine production by dexamethasone and granulocyte-macrophage colony-stimulating factor after stimulation by Aspergillus conidia or lipopolysaccharide. Cytokine *19*, 14–20.

Khalil, A.A., Mueller, S., Foddis, M., Mosch, L., Lips, J., Przesdzing, I., Temme, S., Flögel, U., Dirnagl, U., and Boehm-Sturm, P. (2019). Longitudinal 19F magnetic resonance imaging of brain oxygenation in a mouse model of vascular cognitive impairment using a cryogenic radiofrequency coil. MAGMA *32*, 105–114.

Khanna, N., Stuehler, C., Lünemann, A., Wójtowicz, A., Bochud, P., and Leibundgut-Landmann, S. (2016). Host response to fungal infections – how immunology and host genetics could help to identify and treat patients at risk. Swiss Med. Wkly. *146*, w14350.

Krenke, R., and Grabczak, E.M. (2011). Tracheobronchial manifestations of Aspergillus infections. ScientificWorldJournal *11*, 2310–2329.

Liang, S., Dresselaers, T., Louchami, K., Zhu, C., Liu, Y., and Himmelreich, U. (2017). Comparison of different compressed sensing algorithms for low SNR19F MRI applications—imaging of transplanted pancreatic islets and cells labeled with perfluorocarbons. NMR Biomed. *30*, e3776.

Liang, S., Louchami, K., Holvoet, B., Verbeke, R., Deroose, C.M., Manshian, B., Soenen, S.J., Lentacker, I., and Himmelreich, U. (2018). Tri-modal in vivo imaging of pancreatic islets transplanted subcutaneously in mice. Mol. Imaging Biol. *20*, 940–951.

Lin, S.-J., Schranz, J., and Teutsch, S.M. (2001). Aspergillosis case-fatality rate: systematic review of the literature. Clin. Infect. Dis. *32*, 358–366.

Margalit, A., and Kavanagh, K. (2015). The innate immune response to *Aspergillus fumigatus* at the alveolar surface. FEMS Microbiol. Rev. *39*, 670–687.

Massam, J., Bitnun, A., Solomon, M., Somers, G.R., Guerguerian, A.M., Van Wylick, R., and Waters, V. (2011). Invasive aspergillosis in cystic fibrosis: a fatal case in an adolescent and review of the literature. Pediatr. Infect. Dis. J. *30*, 178–180.

Mccormick, A., Loeffler, J., and Ebel, F. (2010). *Aspergillus fumigatus*: contours of an opportunistic human pathogen. Cell. Microbiol. *12*, 1535–1543.

Nawada, R., Amitani, R., Tanaka, E., Niimi, A., Suzuki, K., Murayama, T., and Kuze, F. (1996). Murine model of invasive pulmonary aspergillosis following an earlier stage, noninvasive Aspergillus infection. J. Clin. Microbiol. *34*, 1433–1439.

Poelmans, J., Hillen, A., Vanherp, L., Govaerts, K., Maertens, J., Dresselaers, T., Himmelreich, U., Lagrou, K., and Vande Velde, G. (2016). Longitudinal, in vivo assessment of invasive pulmonary aspergillosis in mice by computed tomography and magnetic resonance imaging. Lab. Invest. *96*, 692–704.

Poelmans, J., Himmelreich, U., Vanherp, L., Zhai, L., Hillen, A., Holvoet, B., Belderbos, S., Brock, M., Maertens, J., Velde, G.V., and Lagrou, K. (2018). A multimodal imaging approach enables in vivo assessment of antifungal treatment in a mouse model of invasive pulmonary aspergillosis. Antimicrob. Agents Chemother. *62*, e00240–18.

Roilides, E., Katsifa, H., and Walsh, T.J. (1998). Pulmonary host defences against *Aspergillus fumigatus*. Res. Immunol. *149*, 454–465, discussion 523-4.

Rolle, A.-M., Hasenberg, M., Thornton, C.R., Solouk-Saran, D., Männ, L., Weski, J., Maurer, A., Fischer, E., Spycher, P.R., Schibli, R., et al. (2016). ImmunoPET/MR imaging allows specific detection of *Aspergillus fumigatus* lung infection in vivo. Proc. Natl. Acad. Sci. U S A *113*, E1026–E1033.

Ruiz-Cabello, J., Barnett, B.P., Bottomley, P.A., and Bulte, J.W.M. (2011). Fluorine (19F) MRS and MRI in biomedicine. NMR Biomed. *24*, 114–129.

Saini, S., Korf, H., Liang, S., Verbeke, R., Manshian, B., Raemdonck, K., Lentacker, I., Gysemans, C., De Smedt, S.C., and Himmelreich, U. (2019). Challenges for labeling and longitudinal tracking of adoptively transferred autoreactive T lymphocytes in an experimental type-1 diabetes model. MAGMA *32*, 295–305.

Sales-campos, H., Tonani, L., Regina, M., and Kress, V.Z. (2013). The immune interplay between the host and the pathogen in *Aspergillus fumigatus* lung infection 2. *Aspergillus fumigatus* virulence factors. Biomed. Res. Int. *2013*, 1–14.

Schwarz, S., Wong, J.E., Bornemann, J., Hodenius, M., Himmelreich, U., Richtering, W., Hoehn, M., Zenke, M., and Hieronymus, T. (2012). Polyelectrolyte coating of iron oxide nanoparticles for MRI-based cell tracking. Nanomedicine *8*, 682–691.

Shaikh, S., Verma, H., Yadav, N., Jauhari, M., and Bullangowda, J. (2012). Applications of steroid in clinical practice: a review. ISRN Anesthesiol. *2012*, 1–11.

Srinivas, M., Boehm-Sturm, P., Figdor, C.G., de Vries, I.J., and Hoehn, M. (2012). Labeling cells for in vivo tracking using19F MRI. Biomaterials *33*, 8830–8840.

Srinivas, M., Cruz, L.J., Bonetto, F., Heerschap, A., Figdor, C.G., and de Vries, I.J.M. (2010a). Customizable, multi-functional fluorocarbon nanoparticles for quantitative in vivo imaging using19F MRI and optical imaging. Biomaterials *31*, 7070–7077.

Srinivas, M., Heerschap, A., Ahrens, E.T., Figdor, C.G., and de Vries, I.J.M. (2010b). 19F MRI for quantitative in vivo cell tracking. Trends Biotechnol. *28*, 363–370.

Stephens-Romero, S.D., Mednick, A.J., and Feldmesser, M. (2005). The pathogenesis of fatal outcome in murine pulmonary aspergillosis depends on the neutrophil depletion strategy. Infect. Immun. *73*, 114–125.

Stergiopoulou, T., Meletiadis, J., Roilides, E., Kleiner, D.E., Schaufele, R., Roden, M., Harrington, S., Dad, L., Segal, B., and Walsh, T.J. (2007). Host-dependent patterns of tissue injury in invasive pulmonary aspergillosis. Am. J. Clin. Pathol. *127*, 349–355.

Stoll, G., Basse-Lüsebrink, T., Weise, G., and Jakob, P. (2012). Visualization of inflammation using 19F-magnetic resonance imaging and perfluorocarbons. Wiley Interdiscip. Rev. Nanomed. Nanobiotechnol. *4*, 438–447.

Temme, S., Bönner, F., Schrader, J., and Flögel, U. (2012). 19F magnetic resonance imaging of

endogenous macrophages in inflammation. Wiley Interdiscip. Rev. Nanomed. Nanobiotechnol. *4*, 329–343.

van Heeswijk, R.B., Pellegrin, M., Flögel, U., Gonzales, C., Aubert, J.-F., Mazzolai, L., Schwitter, J., and Stuber, M. (2015). Fluorine MR imaging of inflammation in atherosclerotic plaque in vivo. Radiology *275*, 421–429.

Vanherp, L., Poelmans, J., Hillen, A., Govaerts, K., Belderbos, S., Buelens, T., Lagrou, K., Himmelreich, U., and Vande Velde, G. (2018). Bronchoscopic fibered confocal fluorescence microscopy for longitudinal in vivo assessment of pulmonary fungal infections in free-breathing mice. Sci. Rep. *8*, 3009.

Waiczies, H., Lepore, S., Janitzek, N., Hagen, U., Seifert, F., Ittermann, B., Purfürst, B., Pezzutto, A., Paul, F., Niendorf, T., and Waiczies, S. (2011). Perfluorocarbon particle size influences magnetic resonance signal and immunological properties of dendritic cells. PLoS One *6*, 1–9.

Wang, F., Zhang, C., Jiang, Y., Kou, C., Kong, Q., Long, N., Lu, L., and Sang, H. (2017). Innate and adaptive immune response to chronic pulmonary infection of hyphae of *Aspergillus fumigatus* in a new murine model. J. Med. Microbiol. *66*, 1400–1408.

Wang, Y., Chen, L., Liu, X., Cheng, D., Liu, G., Liu, Y., Dou, S., Hnatowich, D.J., and Rusckowski, M. (2013). Detection of *Aspergillus fumigatus* pulmonary fungal infections in mice with99mTc-labeled MORF oligomers targeting ribosomal RNA. Nucl. Med. Biol. *40*, 89–96.

Woodruff, C.A., and Hebert, A.A. (2002). Neonatal primary cutaneous aspergillosis: case report and review of the literature. Pediatr. Dermatol. *19*, 439–444.

Wu, Y.L., Ye, Q., Foley, L.M., Hitchens, T.K., Sato, K., Williams, J.B., and Ho, C. (2006). In situ labeling of immune cells with iron oxide particles: an approach to detect organ rejection by cellular MRI. Proc. Natl. Acad. Sci. U S A. *103*, 1852–1857.

Zhang, X., He, D., Gao, S., Wei, Y., and Wang, L. (2019). *Aspergillus fumigatus* enhances human NK cell activity by regulating M1 macrophage polarization. Mol. Med. Rep. *20*, 1241–1249.

Zhong, J., Narsinh, K., Morel, P.A., Xu, H., and Ahrens, E.T. (2015). In vivo quantification of inflammation in experimental autoimmune encephalomyelitis rats using fluorine-19 magnetic resonance imaging reveals immune cell recruitment outside the nervous system. PLoS One *10*, 1–13.

ISCI, Volume *20*

Supplemental Information

Longitudinal *In Vivo* Assessment of Host-Microbe Interactions in a Murine Model of Pulmonary Aspergillosis

Shweta Saini, Jennifer Poelmans, Hannelie Korf, James L. Dooley, Sayuan Liang, Bella B. Manshian, Rein Verbeke, Stefaan J. Soenen, Greetje Vande Velde, Ine Lentacker, Katrien Lagrou, Adrian Liston, Conny Gysemans, Stefaan C. De Smedt, and Uwe Himmelreich

Supplementary figures

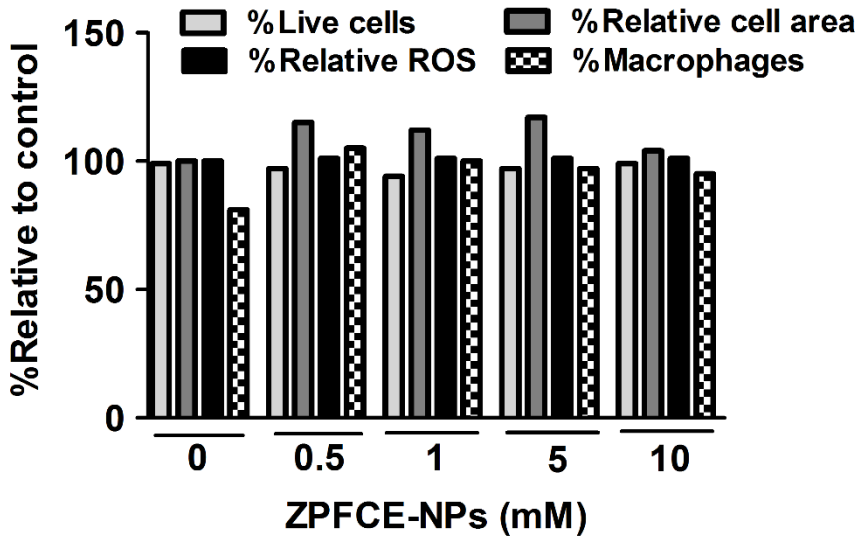

Figure S1. ZPFCE-NP labeling did not show any biological alteration of macrophages, Related to Figures 1 and 2. High-content InCell imaging was performed to evaluate potential cellular toxicity for macrophages upon ZPFCE-NP labeling. Histograms revealed the relative level of cell viability, cell area, formation of mitochondrial reactive oxygen species (ROS) and percentage of macrophages in the total population of immune cells exposed to 0, 0.5, 1, 5, and 10mM of ZPFCE-NPs. Data are represented as mean± SEM of the untreated control values. No statistically significant differences were detected.

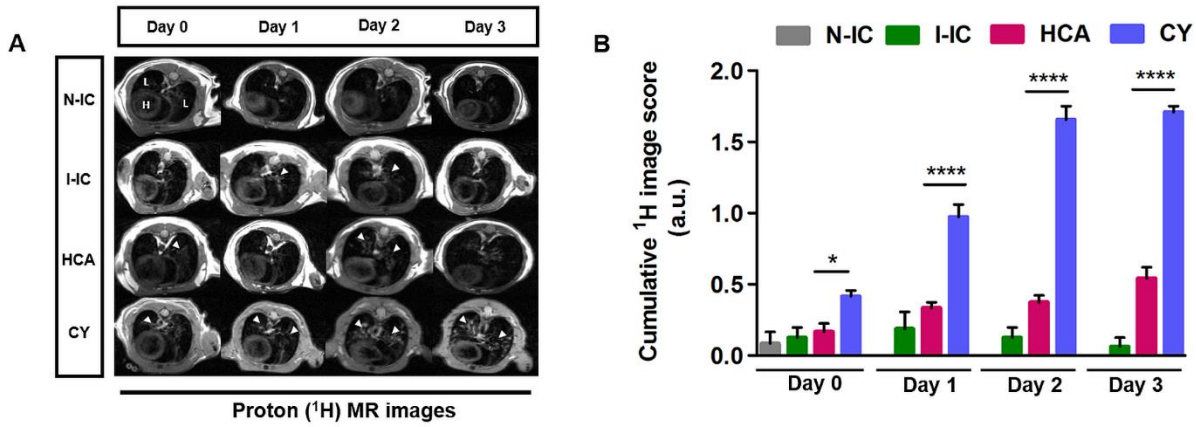

Figure S2. ***In vivo*** **quantification of anatomical changes using ^{1}H MR imaging confirms infection (IPA) and shows lesion development in immunocompromised mice, Related to Figure 3. (A)** ^{1}H MR images were acquired before ^{19}F MRI acquisition using a dual-tuned MR coil. ^{1}H MRI images were acquired daily from the day of infection for three days. Lesions caused by *A. fumigatus* infection are seen as hyperintense (bright) regions (arrow). **(B)** Quantitative estimation of lung lesion development was performed based on the image signal intensities by applying cumulative image scoring method. (N-IC: Non-infected immunocompetent group, *n*=3; I-IC: Infected-immunocompetent group, *n*=4; HCA: Hydrocortisone acetate treated group, *n*=5; CY: Cyclophosphamide treated group, *n*=6). Data represented as mean±SEM. ($*$ $p<0.05$, ****$P<0.0001$).

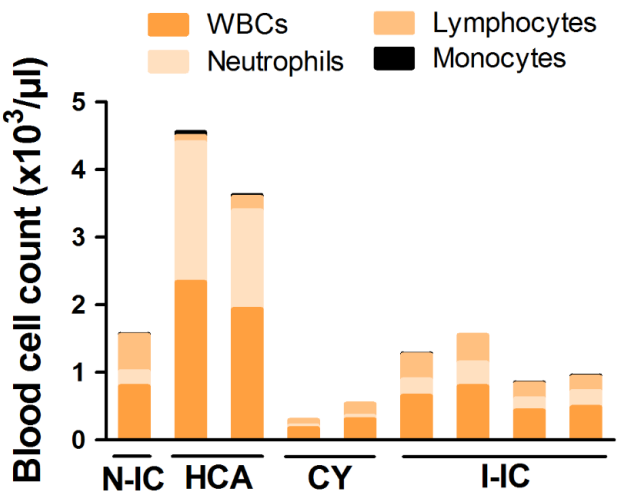

Figure S3. Differential blood immune cell counting depicts patrolling immune cells in all murine groups, Related to Figures 3 and 5. Samples from peripheral blood pool was analyzed for individual mice after cardiac puncturing. Blood samples were collected from different groups on the experimental end-point at day 3. Numbers of white blood cells (WBCs), neutrophils, lymphocytes and monocytes were measured and represented for individual animal.

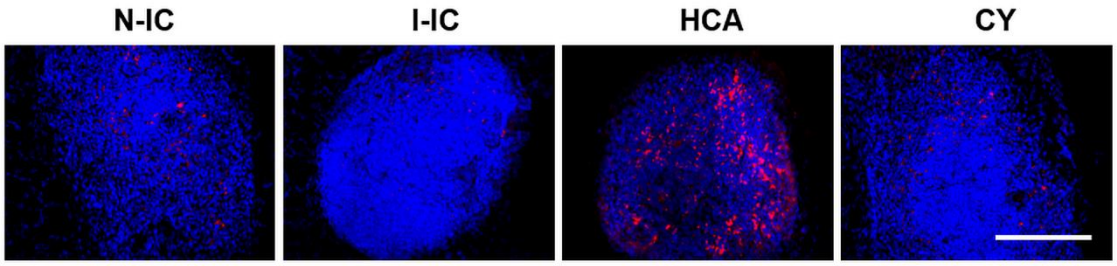

Figure S4. Visualization of ZPFCE-NPs in cervical lymph nodes confirms *in vivo* ^{19}F MRI assessment for all mice groups, Related to Figure 3C. Fluorescent microscopy was performed on cryo-sectioned cervical lymph nodes where high accumulation of ZPFCE-NPs in the lymph nodes was shown in HCA group compared to other groups after animals have been sacrificed on day 3, after infection. Scale bar 100µm. Stainings: Blue=DAPI, Red=ZPFCE-NPs.

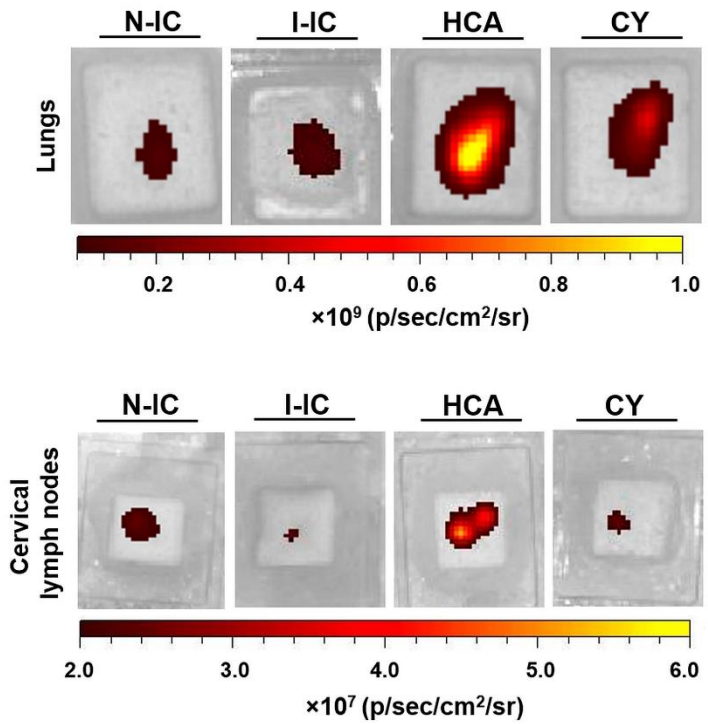

Figure S5. ***Ex vivo*** **fluorescence imaging of lungs and cervical lymph nodes using IVIS Spectrum system confirms ^{19}F MRI, Related to Figures 3 and 4.** Fluorescence images on the cryopreserved OCT-embedded lungs and cervical lymph nodes from all groups of mice were performed after the experimental end-point, three days post-infection. The scale bar represents fluorescence signal intensity. High signal intensities were detected in the lungs and lymph nodes of HCA-treated mice, confirming accumulation of ZPFCE-NP-labeled immune cells.

Transparent method section

Animals

For the *in vitro* labeling experiments, macrophages were isolated from the peritoneum of C57/BL6 female mice (8-9 week-old). Female OT-II mice (6-8-week-old) bearing the MHCII-restricted T cell receptor (TCR) for $OVA_{323–339}$ were bred in house. For *in vivo* experiments, 10-week-old male Balb/c mice (Janvier, Le Genest, France) were housed in KU Leuven animal housing facility with free access to food and water.

All animal experiments were approved by the Ethical Committee of KU Leuven and were conducted according to the Belgian (Royal Decree of 29 May 2013), Flemish (Decision of the Flemish Government to adapt the Royal Decree of 29 May 2013, 17 February 2017) and European (Directive 2010/63/EU) regulations on the protection of animals used for scientific purposes.

Synthesis of fluorinated Zonyl-PFCE nanoparticles

The synthesis of biochemically inert perfluoro-15-crown-5-ether (PFCE) nanoparticles consisting of a PFCE liquid core emulsified by a monolayer of phospholipids was performed as described previously (Dewitte et al., 2013). The fluorosurfactant Zonyl® FSP (Du Pont, Delaware, USA) was incorporated in the lipid shell of PFCE nanoparticles, obtaining nanoparticles with an average size of 280nm. For the *in vitro* and *in vivo* experiments, ZPFCE-NPs were coupled with either Cholestryl BODIPY® FLC12 or DiR fluorescent dye (both from Molecular Probes, Invitrogen, Merelbeke, Belgium).

In vitro labeling of macrophages using ZPFCE nanoparticles

For *in vitro* labeling, cells were incubated with ZPFCE-NPs at fluorine concentration of 0.5, 1 and 10mM for 1h at 37°C in 5% CO2 in ultra-low attachment plates (Corning Costar, Kennebunk, ME, USA). For positive selection of labeled macrophages, cells were analyzed for surface marker expression after pre-incubation with the Fc receptor blocking antibody anti-CD16/CD32 (eBioscience, San Diego, CA, USA) and staining using anti-F4/80 and anti-CD11/b (eBioscience, San Diego, CA, USA) to perform quantitative flow cytometric analyses.

Toxicological assay on ZPFCE-NP labeled macrophages

Primary macrophages were labeled with different concentrations of ZPFCE-NPs. Surface staining with anti-F4/80 (eBiosciences) was performed to identify macrophages by microscopic analysis. Following exposure to nanoparticles, immune cells were stained to assess cell viability, cytoskeletal changes and oxidative stress. Data analysis was performed using a high-content InCell 2000 analyzer (GE Healthcare Life Sciences, Diegem, Belgium) as previously described (Manshian et al., 2014)**.**

Determination of cytokine secretion by ZPFCE-NP labeled macrophages

For cytokine measurement, ZPFCE-NP labeled macrophages were co-cultured in the presence or absence of 1µg/mL lipopolysaccharides (Sigma Aldrich, Overijse, Belgium) for 24h. Supernatants were collected and measurements of IL-10, IL-1beta and TNF-alpha were performed using a customized MSD V-PLEX mouse proinflammatory kit (Mesoscale, Maryland, USA). Readings were performed using a MESO QuickPlex SQ120 plate reader (Mesoscale, Maryland, USA).

In vitro adaptive immune test on ZPFCE labeled macrophages

Splenocytes from OTII transgenic mice were homogenized and negative selection of purified total CD4+ T cells was performed using a cocktail of antibodies for CD16/CD32, CD11b, CD11c, B220, MHC-II and CD8 markers. Contaminating, bead-bound cells were removed using sheep-anti-rat IgG paramagnetic beads, according to the manufacture's specifications (Dynabeads, Invitrogen Merelbeke, Belgium). Purity of samples (>95%) was routinely assessed by flow cytometry. Purified OTII-transgenic CD4+ T cells were co-incubated with ZPFCE-NP labeled macrophages in a 96 well plate together with variable doses of anti-TCR b5.1/b5.2 (OTII) peptide at concentrations of 0, 0.1, 1, 10μg/ml for 1-3 days at 37°C under 5% CO_2 for 1h. To prevent non-specific binding all surface stains were performed in the presence of anti-CD16/CD32. For macrophages, the antibodies F4/80-PerCPCy5.5, CD45-APC-eFluor780 and CD11b-eFluor450 were used. To stain T cells, CD44-FITC, TCRb5.1/5.2-PE, CD62L-Per CPCy5.5, CD69-PECy7 and CD4-eFluor450 were used to assess effector, memory and naïve CD4+ T cell subsets using flow cytometry. All antibodies were purchased from eBioscience (San Diego, CA, USA).

Murine models of invasive pulmonary aspergillosis

To develop a non-neutropenic IPA model, mice were injected subcutaneously (s.c.) with 9mg hydrocortisone acetate per 25g body weight (Sigma-Aldrich, USP, Overijse, Belgium) one and three days before inoculation with *A. fumigatus* (HCA group, *n*=9). To induce neutropenia, 200mg kg^{-1} body weight cyclophosphamide (Sigma-Aldrich, USP, Overijse, Belgium) was injected intraperitoneally (i.p.) one and three days before inoculation with *A. fumigatus* (CY group, *n*=9). Infected immunocompetent mice (I-IC group, *n*=4) and non-infected immunocompetent mice (N-IC, *n*=3) were included as control groups.

The Fluc^{+} *A. fumigatus* strain 2/7/1 was generously provided by M. Brock (School of Life Sciences, University of Nottingham, UK). The strain was cultured and conidia were harvested using a previously described protocol (Poelmans et al., 2016). On day of infection (day 0), HCA and infected immunocompetent groups (I-IC group, n=4) were intranasally instilled with 1×10^{6} spores. The CY group was inoculated with 5×10^{5} spores based on the protocol described previously (Poelmans et al., 2016). ZPFCE-NPs were administered via tail vein 1h prior to MRI acquisition on day 0 and day 1. On the day of inoculation (day 0), MRI experiments were performed on all mice groups 4h after the administration of spores. All murine groups were monitored for weight loss and posture changes starting from day 0 to detect onset of disease symptoms and to define the humane end-points.

Longitudinal in vivo fluorine (^{19}F) magnetic resonance imaging

Animals were anesthetized by intraperitoneal (i.p.) injections of ketamine (45-60 mg kg^{-1}, Nimatek, Eurovet animal health, Bladel, The Netherlands) and Medetomidine (0.6-0.8 mg kg^{-1}, Domitor, The Orion Pharma, Espoo, Finland) solution. *In vivo* longitudinal follow-up of all murine groups was performed using ^{1}H and ^{19}F MRI on a 9.4T preclinical MRI scanner (Bruker Biospec 94/20, Ettlingen, Germany). After the MR acquisition, injections of atipamezole (Antisedan, The Orion Pharma, Espoo, Finland) were administered i.p. to reverse the effects of anesthesia. Throughout the MR imaging experiments, body temperature and respiration rate of the animals were monitored and maintained to 37°C and 60-80 min^{-1}, respectively.

A purpose-built dual-tuned radio frequency surface coil was used to acquire fluorine and ^{1}H MR images. For all *in vivo* MRI experiments, 2D RARE (Rapid Acquisition with Relaxation Enhancement) MRI was performed using the following acquisition parameters: ^{1}H MRI, repetition time (TR) = 3500ms, echo time (TE) = 6.12ms, spatial resolution = 0.156mm×0.156mm, slice thickness = 1mm. For ^{19}F MRI, TR = 5388ms, TE = 6.11ms, spatial

resolution = 1.25mm×1.25mm, slice thickness = 2mm were used. A reference tube containing 30mM of ZPFCE-NPs embedded in agar was placed next to the abdomen of the animal during the MR acquisition to allow quantification of fluorine atoms. For both ^{1}H and ^{19}F MR images, data were acquired with the same localization (placement, orientation of slice packages).

Quantification of ^{19}F MR signal and data processing

Prior to the MR signal quantification, images were reconstructed using the Paravison 5.1 software (Bruker Biospin, Ettlingen, Germany). For post processing, MR images were exported to the MeVislab software version 2.6.1 (MeVis Medical Solutions AG, Bremen, Germany). Gaussian smoothing was applied to the ^{19}F MR images. Before masking the fluorine images, interval thresholding was performed by applying a value higher than the background noise. Masked ^{19}F MR images were rescaled to the same matrix size as the ^{1}H MR images before superimposing them over each other. To calculate the amount of fluorine atoms/voxel, the processed ^{19}F MR images were analyzed slice-wise using the Fiji software, version 1.49a (South Carolina, USA) by drawing the region of interests on the fluorine hot spots in the lungs and the lymph node regions, which were identified based on the anatomical ^{1}H MR images. For quantification, regions were compared with the reference tube that contained 30mM ZPFCE-NPs. Cumulative ^{1}H image scoring was performed on ^{1}H images of all murine groups from day 0 to day 3. Based on the visual observations, lung lesions were identified and a scoring system was used to assign a value for the quantification of signal intensities corresponding to the disease development as described previously (Petraitiene et al., 2002; Petraitis et al., 2003).

Ex vivo bioluminescence imaging

On day 3, the animals were euthanized and the lungs were inflated with 0.5ml D-luciferin (7.5mg) (Promega, Leiden, The Netherlands) by inserting a 22-gauge catheter (Terumo, Heverlee, Belgium) into the trachea. The lungs were immediately placed into the flow chamber

to perform *ex vivo* BLI acquisitions on the IVIS Spectrum imaging system (Perkin Elmer, Massachusetts, USA). Data were analyzed using Living Image® software version 4.5.5 (Perkin Elmer, Massachusetts, USA).

Differential white blood cell measurements

For the differential blood cell counting, mice were euthanized under deep terminal anesthesia and blood was withdrawn using a 25-gauge needle (Terumo, Heverlee, Belgium) from the left ventricles of the beating heart through cardiac puncturing. Total collected blood volume was 0.3 ml from each mouse. To prevent coagulation of blood, 30µl of tri-sodium citrate, 3.8% w/v (VWR, Belgium) was added to the blood collection tubes. Blood cell counts were performed on an ADVIA®2120i hemocytometer, version 5.4 (Siemens Healthcare, GmbH, Erlangen, Germany).

Colony-forming unit (CFU) measurements

After the *ex vivo* BLI acquisition, the right lung lobes were collected in 600µl PBS and homogenized to obtain suspensions of lung tissue. Lung homogenates were plated on Sabouraud agar, followed by an incubation period of 2-3 days at 30°C for manual counting of CFUs.

Flow cytometry and microscopy

Flow cytometry acquisitions were performed on a Gallios™ flow cytometer (Beckman Coulter, Brea, California, USA). For the data analyses, a FlowJo software, version 10.4.2 (FlowJo LLC, Ashland, Oregon, USA) was used. Microscopic images were acquired using a confocal microscope (Nikon, Tokyo, Japan) and analyzed using Fiji software, version 1.49a (South Carolina, USA).

Ex vivo optical imaging of lungs and cervical lymph nodes

Ex vivo fluorescence imaging was performed on the lungs and cervical lymph nodes (LN) of all animals using the IVIS Spectrum imaging system (Perkin Elmer Massachusetts, USA). For the acquisition of data, parameters used are as following: exposure time = 10sec, 740nm excitation and 800nm emission filters with medium binning. Data analysis was performed using the Living Image® software, version 4.5.5 (Perkin Elmer, Massachusetts, USA).

Histology and immunohistochemistry

Right lung lobes were fixed in 4% PFA and embedded in paraffin. For visualization of fungi, lungs were sectioned (5µm) and stained with Periodic acid-Schiff (PAS) agent as described (Poelmans et al., 2016). Brightfield images were acquired using ZEISS Axio Scan.Z1 Digital Slide Scanner (Carl Zeiss, Oberkochen, Germany). For immunoflurosence, left lung lobes were fresh frozen in OCT (optimum cutting temperature) formulation and cryosections (11µm) were fixed in 4% paraformaldehyde and stained according to manufacturer's protocol. For staining of the sections following monoclonal antibodies were used: GR1 (RB6-8C5, eBioscience), CD11b (M1/70, Biolegend), CD11c biotin (N418, eBioscience). For the staining of immune cells, the following detection antibodies were used: Donkey anti-Rat 488, Streptavidin 546, (all from Molecular Probes). Images were acquired using a EVOS FL Auto 2 microscope (Fisher Scientific, Merelbeke, Belgium).

Statistical analysis

For statistical analyses, One-way and Two-way ANOVA tests were performed together with Bonferroni multiple comparison test to compare the different animal groups using the GraphPad Prism software®, version 5.04 (La Jolla, CA, USA).

Supplemental references

Dewitte, H., Geers, B., Liang, S., Himmelreich, U., Demeester, J., De Smedt, S.C., Lentacker, I., 2013. Design and evaluation of theranostic perfluorocarbon particles for simultaneous antigen-loading and19F-MRI tracking of dendritic cells. J. Control. Release 169, 141–149.

Manshian, B.B., Moyano, D.F., Corthout, N., Munck, S., Himmelreich, U., Rotello, V.M., Soenen, S.J., 2014. High-content imaging and gene expression analysis to study cell-nanomaterial interactions: The effect of surface hydrophobicity. Biomaterials 35, 9941–9950.

Petraitiene, R., Petraitis, V., Groll, A.H., Sein, T., Schaufele, R.L., Francesconi, A., Bacher, J., Avila, N.A., Walsh, T.J., 2002. Antifungal efficacy of caspofungin (MK-0991) in experimental pulmonary aspergillosis in persistently neutropenic rabbits: Pharmacokinetics, drug disposition, and relationship to galactomannan antigenemia. Antimicrob. Agents Chemother. 46, 12–23.

Petraitis, V., Petraitiene, R., Sarafandi, A. a, Kelaher, A.M., Lyman, C. a, Casler, H.E., Sein, T., Groll, A.H., Bacher, J., Avila, N. a, Walsh, T.J., 2003. Combination therapy in treatment of experimental pulmonary aspergillosis: synergistic interaction between an antifungal triazole and an echinocandin. J. Infect. Dis. 187, 1834–1843.

Poelmans, J., Hillen, A., Vanherp, L., Govaerts, K., Maertens, J., Dresselaers, T., Himmelreich, U., Lagrou, K., Vande Velde, G., 2016. Longitudinal, in vivo assessment of invasive pulmonary

aspergillosis in mice by computed tomography and magnetic resonance imaging. Lab. Invest. 96, 692–704.